Molecular dynamics study of ion impact phenomena

1994 J. Phys.: Condens. Matter 6 7833

(http://iopscience.iop.org/0953-8984/6/38/020)

J. Phys.: Condens. Matter 6 (1994) 7833–7846. Printed in the UK

Molecular dynamics study of ion impact phenomena

N A Marks, D R McKenzie and B A Pailthorpe
School of Physics, University of Sydney, Broadway, NSW 2006, Australia

Received 18 April 1994

Abstract. We use molecular dynamics to study the phenomena occurring after ion impact. The simulations are two dimensional, the target contains approximately 5000 nickel atoms and the impacting ions have an energy in the range 100–1000 keV. The phenomena observed include focused collision sequences, sputtering and a thermal spike. The focused collision sequences transport much of the ion's energy away from the impact site and significantly reduce the size of the thermal spike. In an analogous process to Čerenkov radiation, it is shown that the focused collision sequences travel at supersonic speeds and lose energy via the production of sound waves. When an electron–phonon interaction is included the phenomena are slightly damped, but their essential features are unchanged.

1. Introduction

The phenomena taking place under the surface of a material following ion bombardment have been the subject of study for many years. These phenomena are important in the understanding of sputtering, radiation damage and the modification of the properties of thin films during growth. The last of these provided the motivation for this study, in particular, the need to know more about the phenomena that produce compressive stress and allow it to be relieved.

The ideas of the focused collision sequence and the thermal spike, for example, are well known [1], and have shaped thinking on ion beam interactions. One of the crucial questions about the focused collision sequence is the energy loss mechanism [2], as this limits its range. The nature of the thermal spike, including its size and time evolution, and the manner in which it is affected by the incident particle energy are also in need of study.

In this paper we study a large two-dimensional array of approximately 5000 atoms using molecular dynamics (MD). MD provides a unique means of studying phenomena with very fine spatial and time resolution, and hence of obtaining information that is difficult or impossible to access experimentally. With a two-dimensional (2D) model we are able to capture the essential physics and gain insights applicable to real 3D systems. The advantages of a 2D simulation, over one performed in 3D, are that for the same computational effort, a considerably larger system can be studied and the phenomena can be visualized much more readily.

2. The model

The MD simulation was performed in two dimensions, and contained approximately 5000 atoms. The atoms interacted via the Lennard-Jones 6–12 pair potential:

$$U_{LJ}(r) = 4\varepsilon\left[\left(\frac{\sigma}{r}\right)^{12} - \left(\frac{\sigma}{r}\right)^{6}\right]$$

0953-8984/94/387833+14$19.50

where ε is the potential well depth, or bond energy, and σ measures the atomic size. For computational efficiency the interactions were truncated at 2.45σ (or 5.49 Å), which lies between the third- and fourth-nearest neighbours. Being a central potential, the Lennard-Jones interaction is suitable for describing close-packed systems, such as the noble gases and many metals. Nickel was chosen as the material of study because it packs in the FCC structure, and has been successfully described in previous MD work by Müller [3] and Chirita [4]. The parameters used, namely

$$\varepsilon_{2D} = 1.32\,\text{eV} \qquad \sigma = 2.24\,\text{Å}$$

are those appropriate for nickel in two dimensions [3], i.e. ε_{2D} is twice the 3D value to preserve the cohesive energy. This choice of ε results in a speed of sound of $12.5\,\text{km s}^{-1}$, somewhat above the experimental value of $6.04\,\text{km s}^{-1}$ [5]. However, this is not of great concern since the phenomena are not sensitive to the numerical value of the velocities.

The simulation consisted of a target 250 Å wide and 110 Å deep, and onto this single atoms were deposited. The upper surface of the target was free while the remaining three edges were fixed. Incident atoms were deposited in the middle of the upper surface and the system was monitored until the disturbances reached the boundary, a time typically 0.25 ps later. The majority of the simulations used a single-crystalline target containing 52 close-packed rows of 100 atoms. In a small number of simulations a polycrystalline target of 4900 atoms was used instead.

2.1. Computational method

Verlet's algorithm [6] was used to numerically integrate the Newtonian equations of motion. The integration timestep was chosen in order that the total energy, i.e. potential plus kinetic energy, was constant. A timestep of order 0.01 fs was typically used. The atomic kinetic energies were used as a measure of the temperature.

Significant savings in execution time were obtained by use of a neighbourhood list of atoms [7], avoiding unnecessary calculations of long-range interactions, which are numerically negligible. Calculation of the list was optimized by subdividing the system into small cells [8]. The execution time scaled linearly with the number of atoms rather than as their square, allowing the study of large systems with comparative ease. On a Fujitsu VP-2200 supercomputer a 0.5 ps simulation of 5200 atoms took approximately ten minutes.

2.2. Damping due to electron–phonon coupling

In a classical MD approach the ions interact with one another via some potential and the presence of the electrons is ignored. However, in many instances the presence of the electrons is important. For example, electronic stopping is the dominant energy loss mechanism for ions in the MeV range. Another example is the electron–phonon interaction, which couples the electron and phonon systems and brings them to equilibrium.

In a thermal spike, the electron–phonon coupling can be important [9], and significant amounts of heat can be conducted from the ions to the electrons, damping the motion of the ions and reducing the temperature of the spike. Finnis and co-workers [10] derived the differential equations governing the transfer of heat between the ion and electron systems. They also proposed a simpler version of the equations suitable for incorporation into a molecular dynamics simulation. They modelled the loss of energy from the ion system to the electrons with a velocity-dependent friction force which applied to each ion. There was

no reverse transfer of energy from the electrons to the ions, but this is not a serious limitation as the electronic thermal conductivity is much greater than the phonon conductivity. This means the electrons conduct heat away much faster than the phonons and hence the electron temperature can be considered constant. The friction force had the following form:

$$F_i = -\alpha m \frac{T_i - T_e}{\sqrt{T_i^2 + (T_e/20)^2}} v_i$$

where i is the ion index, T_i and T_e are the ion and electron temperatures, m is the ion mass and α is a constant dependent on both the material and the electron temperature. The ion temperature was defined using equipartition in two dimensions, i.e. $T_i = mv_i^2/2k$. Isolated atoms, such as the incoming ion or the sputtered atoms, did not experience the frictional force as the derivation applies only to bulk material.

The coefficient αm in the expression above describes the strength of the electron–phonon coupling. A high value of αm implies a strong electron–phonon interaction and *vice versa*. Large differences in αm, and hence the cooling rate, are possible for materials that are otherwise quite similar. For example, the coupling in nickel is some 30 times stronger than in copper, even though they are adjacent in the periodic table. We performed simulations using αm for both nickel and copper to assess the significance of electron–phonon coupling in a thermal spike.

2.3. The distortion parameter δ

In order to identify the region forming the thermal spike it is necessary to have a measure of local distortion in the system. We defined a parameter, δ, which measures the deviation of triplets of atoms from the equilateral arrangement. This exploits the property that, in a perfect close-packed lattice, all the nearest neighbours form equilateral triangles.

Calculating δ is a two-step process. First, a quantity Δ is calculated for each bonded triplet of atoms. The difference of each angle from 60° is found, and summing the three differences gives Δ, the deviation of that triangle from the ideal arrangement. In order that it be a property of an atom and not a triangle, δ is defined as the average of Δ for all the triangles to which the atom belongs. Thus δ is a measure of the local distortion at an atom.

3. Results

We present results for impacts in three systems. In the first we look at impacts onto a crystalline array, in the second onto a polycrystalline array and in the third we revisit the crystalline array and add the effects of electron–phonon coupling. We first consider the crystalline film in the absence of electron–phonon coupling.

Simulations were performed for ion impact energies of 100 eV, 400 eV and 1 keV. In each simulation a single atom was deposited onto the 5200 atom surface, which was initially at 100 K. The simulations show four distinct energy loss mechanisms: focused collision sequences, a sonic wavefront or 'bow wave', sputtering and a molten zone or 'thermal spike'. These processes are shown schematically in figure 1. The dotted lines show the paths of the focused collision sequences, or focusons. These travel at supersonic speeds along the close-packed directions in the crystal. The full black lines show the bow waves,

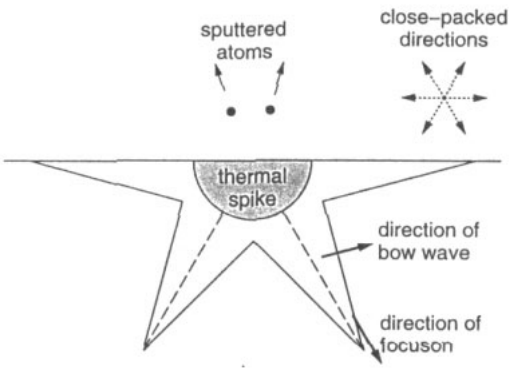

Figure 1. A schematic view showing the four main energy loss mechanisms after ion impact: focused collision sequences, or focusons (dotted lines), bow waves (full lines), thermal spike (grey shading) and sputtering. For clarity the focusons travelling along the surface have not been shown as dotted lines.

which are plane waves and travel at the speed of sound in a direction perpendicular to their wavefront. These bow waves have not, to our knowledge, been previously reported.

The focused collisions sequences and bow waves are best illustrated using diagrams that display the energy of the atoms. This method is used in figures 2 and 3, which show the system at various times after the impact of 100 eV and 1 keV atoms respectively. Atoms with a kinetic energy over 0.2 eV are shown as large circles, while those atoms with a lower energy are shown as small circles. The star-shaped pattern produced by the focusons and bow waves dominates the 1 keV pictures, and is also present for a short time after the 100 eV impact. The energy pattern is symmetric in these simulations because the atom impacted exactly midway between two surface atoms. When other impact parameters are used the symmetry is different, but the essential features remain the same. The thermal spike is not easily seen using this energy picture, and is shown later using the distortion parameter δ instead. We now look at each of the four energy-loss mechanisms in detail.

3.1. Focused collision sequences

Focused collision sequences were first proposed by Silsbee in 1957 [11], and since that time have been extensively studied. Their existence is well supported by experimental work on sputtering of high-Z metals [12, 13], analytical work on self-focusing in linear cascades [14] and small-scale MD work in iron [15].

The central feature of a focused collision sequence is the transfer of energy along a close-packed direction without any attendant flow of matter. The transfer of energy is very efficient, as the mechanics of the collisions produces a strong focusing effect which aligns the collision sequence with the close-packed direction. The manner in which the focuson moves through the crystal is shown in figure 4. The two atoms at the apex are much closer than at equilibrium, and such a close approach produces a large repulsive force. It is this strong interaction that is responsible for the high speed of propagation of the focuson.

The displacement of the atoms along the path of the focuson is only temporary, and figure 4 shows the atoms behind the apex relaxing back to their lattice sites. These atoms retain a small fraction of the energy of the focuson, but the most significant energy loss mechanism is the bow wave, which is discussed below. Continued energy loss eventually

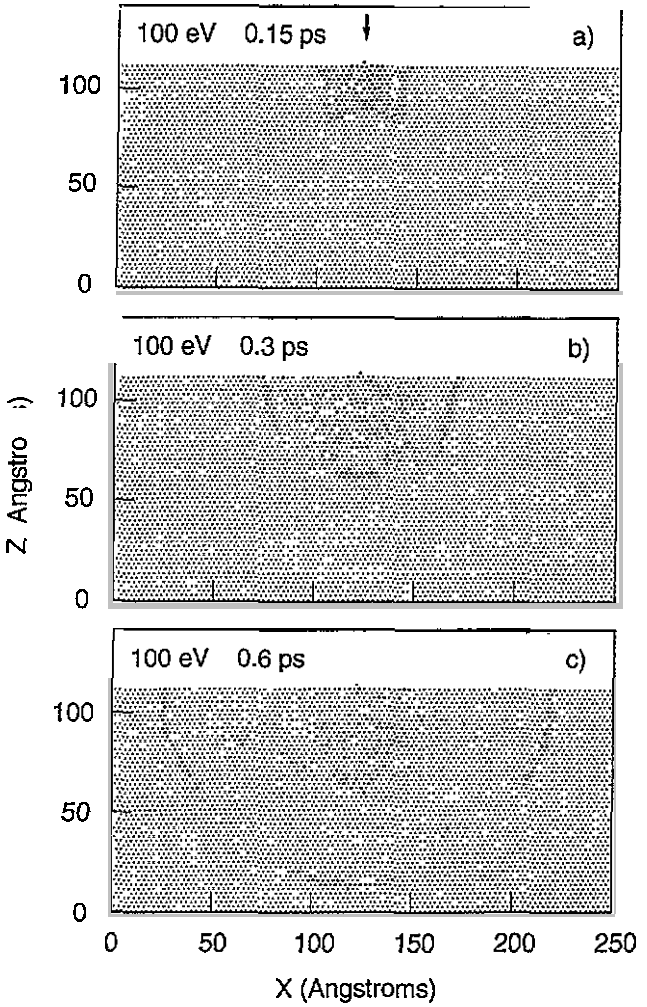

Figure 2. The crystalline system (*a*) 0.15 ps, (*b*) 0.3 ps and (*c*) 0.6 ps after the impact of a 100 eV ion at the position indicated by the arrow. The small circles represent atoms with an energy less than 0.07 eV, while the large circles represent atoms with an energy greater than 0.07 eV.

removes the focuson and this is seen in figure 2(*b*) where the focuson has disappeared after 0.3 ps. The disappearance of the focusons is coincident with their speed slowing to the sound velocity. This shows that a focuson can exist only when it is travelling at supersonic speeds. This observation has not to our knowledge been previously made. The case for focusons being supersonic can be argued as follows. The focuson speed cannot be lower than the speed of sound as even a small amplitude disturbance will travel at the speed of sound along a close-packed chain. Neither can the focuson speed equal the sound velocity because a sound wave would expand with a semicircular wavefront, which is inconsistent with the directed nature of the focuson. Thus for a focuson to exist it is necessary that it travel at supersonic speeds.

Since a focuson is confined to a linear chain of atoms along a close-packed direction, some aspects of its behaviour can be studied with an isolated linear chain. We studied the

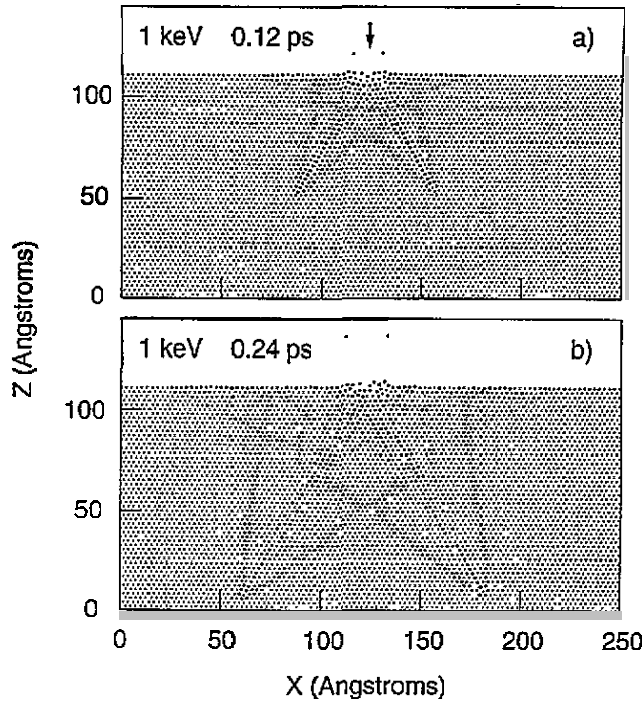

Figure 3. The crystalline system (*a*) 0.12 ps and (*b*) 0.24 ps after the impact of a 1 keV ion at the position indicated by the arrow. The small circles represent atoms with an energy less than 0.2 eV, while the large circles represent atoms with an energy greater than 0.2 eV.

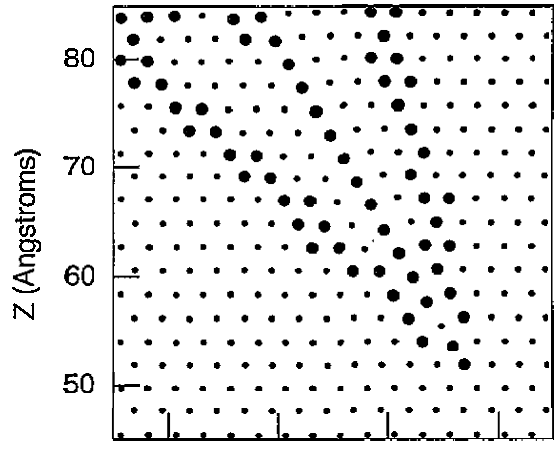

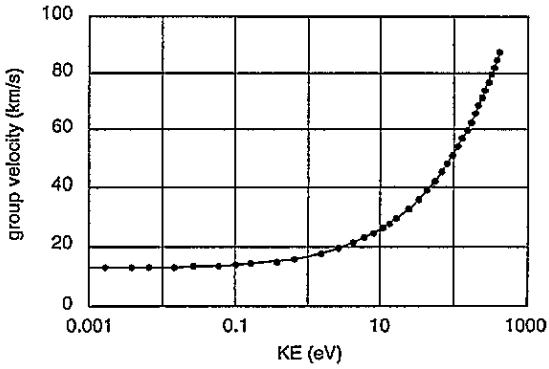

Figure 5. The group velocity of a pulse in a one-dimensional chain as a function of the kinetic energy which initiates the pulse. This curve also describes the relationship between the speed of a focuson and its energy, and shows that focusons are supersonic. Note that the group velocity reduces to 12.5 km s^{-1}, the sound velocity, when the kinetic energy is low.

relationship between the speed of a focuson and its kinetic energy using a one-dimensional simulation containing 100 nickel atoms. Figure 5 shows the dependence of the speed, or group velocity of the pulse, on the kinetic energy of the atom that initiates it. This relationship can be used to determine the amount of energy contained in a focuson simply by measuring its velocity. In the case of the 1 keV impact, the initial velocities of the four focusons are 50, 52, 72 and 75 km s^{-1}. This corresponds to initial kinetic energies of 90, 100, 250 and 275 eV respectively. Thus the focusons receive 715 eV of the original 1 keV.

3.2. Bow waves

As mentioned above, the main way in which the focuson loses energy is via the production of bow waves. The bow waves originate at the focuson tip and travel outwards at the speed of sound. Since the focuson travels at supersonic speeds the two wavefronts form a wedge.

This situation is reminiscent of Čerenkov emission, in which a particle radiates a cone of energy when it exceeds the speed of light in the medium. In the Huygens wavelets treatment of Čerenkov emission, and more generally, bow waves of any kind, the half-angle of the cone (θ) can be calculated using the relationship $\sin\theta = c/v$, where c is the velocity of the bow waves and v is the particle speed. This relationship correctly describes the focuson and bow waves. For example, the focuson in figure 4 has a velocity of $3.2c$ which, when used to calculate θ, gives 18°, the same angle observed in the figure. The expression also implies that θ increases as the focuson loses energy and its speed slows. We see this in figure 3, where the half-angle θ increases from 18° after 0.12 ps to 23° after 0.24 ps.

It is also constructive to examine the bow wave from an atomic viewpoint. At the most fundamental level, energy is transferred from the focuson to the bow wave via interactions between the focuson and the surrounding atoms. The atom at the head of the focuson interacts strongly with two atoms which lie perpendicular to its direction of motion. Both atoms are slightly displaced as the focuson moves through the crystal and this results in a transfer of energy from the focuson to the two perpendicular atoms. It is this transfer of energy in a coherent manner to successive pairs of atoms that forms the bow wave.

In its three-dimensional analogue, the focuson displaces four atoms instead of two and these four atoms are termed the 'focusing ring' [14]. Theoretical descriptions of focused collision sequences view the energy loss process as an energy loss to a succession of these focusing rings. The bow waves should be seen as an alternative view of the same process.

The new feature that the bow waves present is that energy is lost from a focuson in a coherent manner, and that the resulting energy pattern parallels many other phenomena.

3.3. Thermal spike

While the focusons and the bow waves are coherent processes, a significant fraction of energy is lost in an incoherent manner, the initial stages of which cause melting. This molten zone is usually termed a 'thermal spike'. One possible view of the thermal spike is that region in which the atoms have an average kinetic energy comparable to the bond strength ε. However, the kinetic energy of molten atoms oscillates in time, which makes it very difficult to identify the thermal spike using an energy picture. This problem is evident in figure 3, where it is difficult to isolate the thermal spike from the focusons and bow waves.

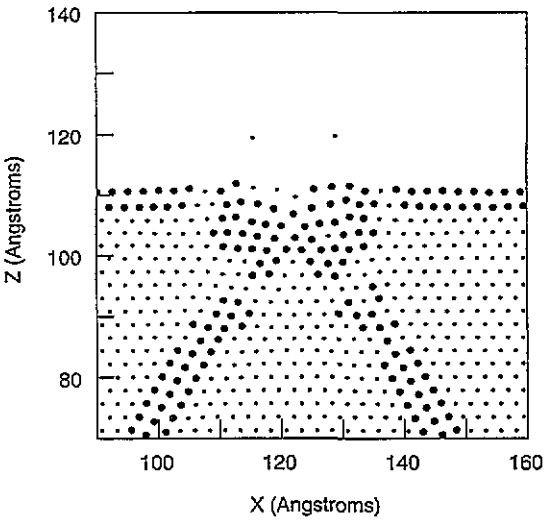

Figure 6. An illustration of a typical thermal spike using the distortion parameter δ. The small circles indicate atoms with δ less than 15°, while the large circles indicate atoms with δ greater than 15°. The semicircular spike is easily distinguished from the lines of distortion caused by the focuson.

To avoid this problem we defined the thermal spike as the region in which local structure was significantly distorted. The distortion was measured using the parameter δ defined earlier, and the atoms were displayed according to the size of δ. Atoms with a value of δ exceeding 15° were shown as large circles, while those atoms with a lower value were shown as small circles. The cutoff of 15° was empirically chosen to identify molten atoms. A typical picture is shown in figure 6, and in this diagram the semicircular thermal spike is easily distinguished from the straight lines that outline the focuson remnant. The bow waves are removed from view as the plane waves are of relatively small amplitude and do not cause a major distortion.

The number of atoms in the thermal spike is shown as a function of time and energy in figure 7. This shows how the disordered region expands to a maximum size, then contracts as the energy flows away and the atoms relax back to an ordered crystalline structure. The expansion of the spike is slow in comparison with the rapid motion of the focusons as the energy in the spike is incoherent.

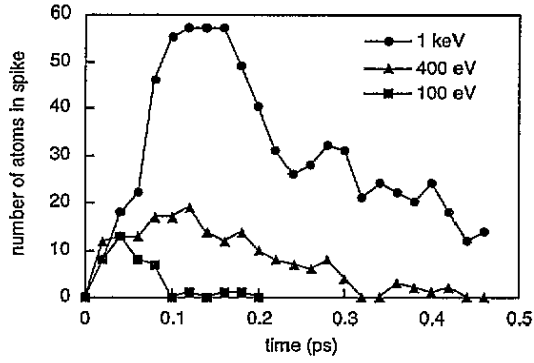

Figure 7. The size of the thermal spike as a function of time for ion energies of 100 eV (square), 400 eV (triangle) and 1 keV (circle).

The number of atoms present in the thermal spike is considerably reduced due to the large amount of energy removed by the focusons. At first one might suppose that a 1 keV ion would produce a thermal spike containing around 1000 atoms with roughly 1 eV apiece. Indeed, if the target were amorphous this may well be a reasonable first approximation. The amount of energy delivered to the thermal spike can be deduced by subtracting the energies contained in the focusons and sputtered atoms from the original ion energy. In the 1 keV impact the sputtered atoms removed 96 eV and, as calculated previously, the focusons contained 715 eV. Thus the energy contained in the thermal spike is less than 200 eV.

In a three-dimensional impact the amount of energy directed into focusons is more variable than in 2D, and is dependent on the incident direction and impact parameter of the ion. Nevertheless, focusons have the potential to dramatically reduce the size and temperature of a thermal spike.

3.4. Sputtering

Sputtering is another means of energy dissipation from the initial impact. No atoms were sputtered by the 100 eV ion, but in both the 400 eV and 1 keV impacts, two atoms were ejected. We compare these results to experimental work on self-sputtering of nickel [16], which found a yield of 0.2 atoms per incident ion at 100 eV, and 2 atoms per incident ion at 1 keV.

In the 1 keV impact the atoms were ejected with energies of 47 and 49 eV, and at angles of 12° and 13° from the normal. Figure 8 shows a detailed view of this event. The small dots show the centre of each atom at previous times. The pictures show that the impacting ion transfers almost all its energy to two surface atoms and that they in turn transfer much of their energy to two atoms each. Thus after 9.0 fs there are four atoms with an energy of approximately 250 eV each. Two of these four atoms are sputtered, but they leave the surface with an energy considerably less than 250 eV due to the collision seen in the final frame.

We note that sputtering is not affected by the thermal spike as the time scales for the two processes differ by an order of magnitude. The sputtered atoms leave the surface just 0.02 ps after impact, at which point the thermal spike is barely discernible. Thus it is a series of rapid localized processes near the surface that give rise to sputtering.

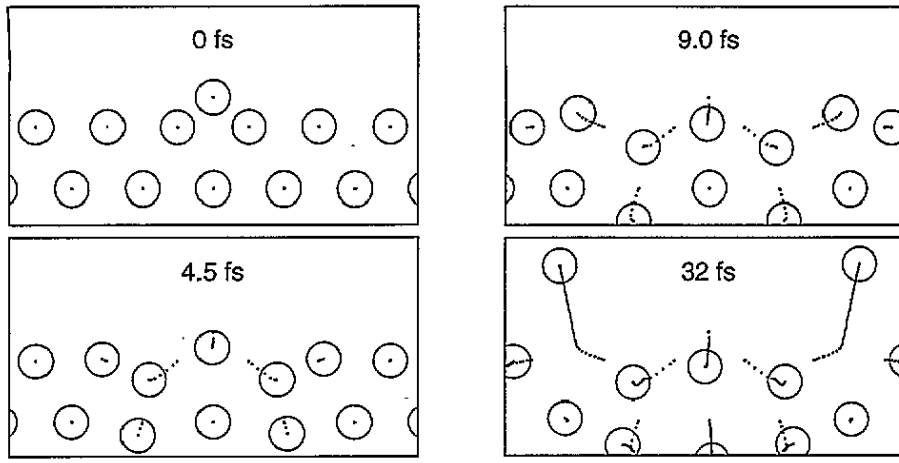

Figure 8. The sequence of collisions which comprise a sputtering event for a 1 keV ion. The small dots show the centre of the atoms at previous times, and the time interval between dots is 0.75 fs.

3.5. Final cooling phase

The final stage of energy loss involves thermal diffusion, and this is seen most clearly in figures 2(*b*) and 2(*c*). Inside the wavefronts lies the diffusing region, where the energy of the atoms is incoherent. With its expansion driven by the temperature gradient, this region continues to expand until all the energy has diffused away. The wavefronts are remnant bow waves and these travel outwards at the speed of sound. Thus the coherent energy propagates away at the speed of sound, while the incoherent energy diffuses away on a much slower time scale. We are unable to observe this final stage of energy loss in the 1 keV case as the time and spatial scales required are excessive.

3.6. Ion impact onto a polycrystalline surface

The results presented thus far are for atoms incident upon a crystalline surface. In this section we demonstrate the effects seen when the target is polycrystalline. A polycrystalline film of 4900 atoms was synthesized by relaxing a square lattice, which is under-coordinated and therefore unstable. As the system relaxed to a lower potential energy much kinetic energy was produced and this was removed by periodically rescaling all atomic velocities to zero. This process was repeated until the temperature had dropped to 300 K. The resulting film (figure 9(*a*)) is considerably less dense than the crystal lattice used previously, and contains many features such as grain boundaries, voids, vacancies and line dislocations.

A 1 keV atom was deposited onto the film, and in figure 9(*b*) the system is shown 0.5 ps after impact. While this picture differs from the crystalline case there are significant similarities, with all of the energy loss mechanisms present.

The presence of only one major focuson illustrates the dependence of focuson generation on the surface structure and impact parameter. The surface is stepped, and in this particular impact a lack of atoms to the right of the impact site damped the focuson travelling downward and to the right. These variations also removed the surface focusons. However, focusons were created at places other than the point of impact. When the original focuson passed through a defect, it initiated a secondary focuson and bow wave which can be seen approximately 20 Å below the surface near the left edge of the disturbance.

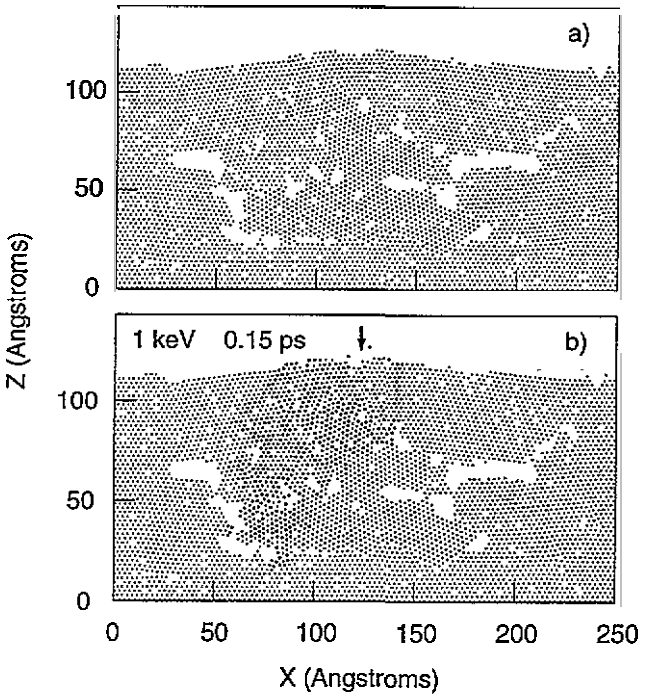

Figure 9. (*a*) The polycrystalline lattice of 4900 atoms. (*b*) The same system 0.5 ps after the impact of 1 keV ion at the position indicated by the arrow. The small circles represent atoms with an energy less than 0.2 eV, while the large circles represent atoms with an energy greater than 0.2 eV.

In comparison with the earlier examples, the bow waves are less well defined as the wavefront is scattered by defects. The wedge about the focuson remains, but inside it there is considerable incoherent energy. This incoherent energy is present far deeper in the film than in the crystalline case and may provide a mechanism for annealing at significant depths. With this being the case, the thermal spike is not the semi-circular region seen before, but has a more complex shape.

As in the single crystal case, two atoms were sputtered by the 1 keV ion. Less energy was removed, however, and the atoms had energies of only 1 and 25 eV. The asymmetry was reflected in the ejection angles too, which were 11° and 50° from the normal respectively. However, since sputtering is such a rapid and localized process, these differences reflect the surface detail, and are not a product of the polycrystalline nature of the target.

3.7. Effect of electron–phonon coupling

To evaluate the significance of electron–phonon coupling we simulated two further 1 keV impacts, one using αm for nickel, the other with αm for copper. As mentioned previously, the coupling in nickel is some 30 times stronger. By using two values of αm that differ so greatly we can gain insight into how the coupling might affect the phenomena in a range of materials. For an electron temperature of 100 K, the coupling constants were [10]

$$\alpha m_{\mathrm{Ni}} = 7.98 \times 10^{-13}\,\mathrm{kg\,s^{-1}} \qquad \alpha m_{\mathrm{Cu}} = 2.49 \times 10^{-14}\,\mathrm{kg\,s^{-1}}.$$

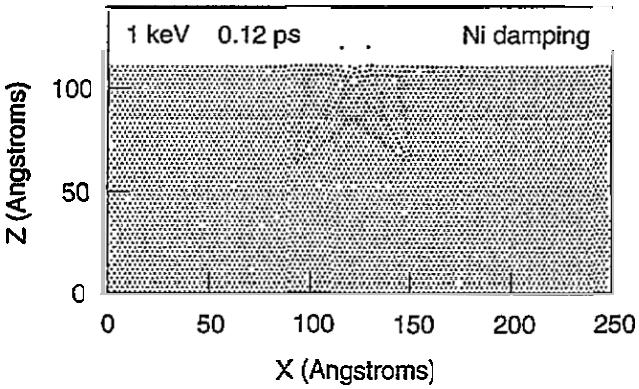

Figure 10. An illustration of the effect of electron–phonon coupling. The parameter for nickel was used and here the system is shown 0.12 ps after the impact of a 1 keV ion. The small circles represent atoms with an energy less than 0.2 eV, while the large circles represent atoms with an energy greater than 0.2 eV.

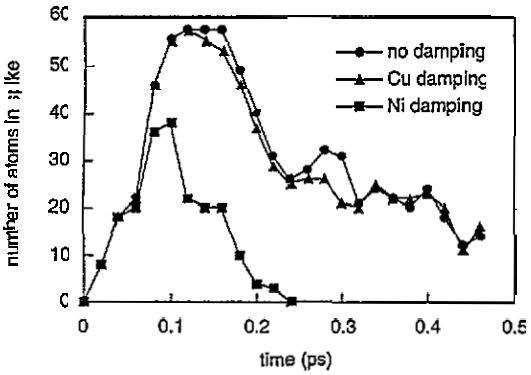

Figure 11. The size of the thermal spike due to a 1 keV ion using different electron–phonon coupling strengths: no coupling (circle), copper parameter (triangle) and nickel parameter (square).

The effect of electron–phonon coupling on a 1 keV impact is shown in figure 10. The coupling was described using αm for nickel and the only difference between this picture and the one in figure 3(a) is the inclusion of the damping. The features seen previously are still present but are noticeably attenuated. The sputtered atoms had energies of 32 and 35 eV (a fall of 30%) and the half-angle θ increased to 20°, which indicates the focuson was slower. The size and duration of the thermal spike were also significantly affected, as figure 11 shows. Not only did the spike have fewer atoms, but the rate at which it contracted was much greater. This accelerated cooling suggests an increased number of defects in a material with a high value of αm. However, the increase in cooling rate would be offset by the reduction in the size of the spike as seen here.

Another effect of the electron damping is the limitation it places on the range of the focuson. In the simulation shown in figure 10, the focusons travelled only 50 Å before they disappeared. However, in the simulation shown in figure 3, the focusons and bow waves were still extremely strong at a depth of 100 Å. Thus the electron–phonon coupling limits the depth to which a material may be modified by focusons.

In contrast, very little damping occurred when the simulation was repeated using αm of copper. Figure 11 shows that the thermal spike is barely affected by the damping and pictures of the focuson and bow waves are essentially identical to those seen in figure 3. Thus, for phenomena in the 1 keV range, the necessity of including electron–phonon effects needs to be evaluated on a case-by-case basis.

4. Discussion and conclusion

In this work we have studied the phenomena occurring after ion impact and have evaluated their relative importance. The kinetic energy of the ion is directed into one of three primary processes: focused collision sequences or focusons, a thermal spike and sputtering. The focusons in turn lose energy via the production of bow waves, a phenomenon we believe to be not previously reported.

Of the three primary energy loss processes, the focusons are the most significant. They remove large amounts of energy from the impact site and carry it away at supersonic speeds. In some instances the focusons travelled over 100 Å. Supersonic speeds are a fundamental property of focusons, as a focuson can exist only when it is travelling faster than sound. The size and duration of thermal spikes are significantly affected by the focusons as the transport of energy away from the impact site is both rapid and efficient. The sputtering process is rapid (0.02 ps), localized and independent of both the focusons and the thermal spike. Electron–phonon coupling damps the system to varying degrees, but the qualitative nature of the phenomena remains unchanged.

Acknowledgments

The authors wish to thank Australian Numerical Simulation and Modelling Services (ANSAMS) for provision of considerable CPU time on their Fujitsu VP-2200. Many helpful discussions with Craig Davis are gratefully acknowledged. Thanks also go to VisLab at The University of Sydney for access to extensive visualization resources. The authors acknowledge financial support by His Royal Highness Prince Nawaf Bin Abdul Aziz through the Science Foundation for Physics within Sydney University.

References

[1] Hofer W O 1991 *Sputtering by Particle Bombardment III* ed R Behrisch and K Wittmaack (Berlin: Springer)
[2] Hofer W O 1991 *Sputtering by Particle Bombardment III* ed R Behrisch and K Wittmaack (Berlin: Springer) p 35
[3] Müller K-H 1987 *J. Appl. Phys.* **62** 1796
[4] Chirita V and Pailthorpe B A 1992 *Thin Solid Films* **208** 149
[5] Weast R C (ed) 1974 *Handbook of Chemistry and Physics, 54th edn* (Cleveland, OH: Chemical Rubber Company) p C47
[6] Verlet L 1967 *Phys. Rev.* **159** 98
[7] Berendson H J C and Van Gunsteren W F 1986 *Molecular Dynamics Simulations of Statistical-Mechanical Systems* ed G Ciccotto and W G Hoover (Amsterdam: North-Holland) p 46
[8] Greengard L 1990 *Comput. Phys.* **4** 142
[9] Flynn C P and Averback R S 1988 *Phys. Rev.* B **38** 7118
[10] Finnis M W, Agnew P and Foreman A J E 1991 *Phys. Rev.* B **44** 567
[11] Silsbee R H 1957 *J. Appl. Phys.* **28** 1246
[12] Szymczak W and Wittmaack K 1980 *Nucl. Instrum. Methods* **170** 341

[13] Linders J, Niedrig H and Sternberg M 1984 *Nucl. Instrum. Methods Phys. Res.* B **2** 649
[14] Robinson M T 1981 *Sputtering by Particle Bombardment I* ed R Behrisch (Berlin: Springer)
[15] Erginsoy C, Vineyard G H and Englert A 1964 *Phys. Rev.* **133** A595
[16] Harrison D E and Magnuson G D 1961 *Phys. Rev.* **122** 1421